Assessment of Performance Variation on the Axial and Radial Forces in Turbopump Configurations for Liquid Rocket Engines

Bernd Wagner[1]*, Julian D. Pauw[2], Lucrezia Veggi[2]

ISROMAC 2017

International Symposium on Transport Phenomena and Dynamics of Rotating Machinery

Maui, Hawaii

December 16-21, 2017

Abstract

In the frame of the KonRAT project, selected topics of turbopump design and operation are considered. In the work package of secondary the following topics are considered systems gap flow, bearing, and seals. Especially the bearings of liquid rocket engines turbopumps are highly loaded due to harsh environment in which they are operating.

Thus, accurate knowledge of the acting radial and axial forces in the nominal operation is necessary for the design of the bearing unit and is subsequently important for safe operation of the turbomachinery. This requires, in turn, an understanding of the flow in the rotor stator cavities, since a pressure distribution and thus forces can be derived therefrom. A program was developed for the calculation of the acting forces. It is generally applicable for different turbopump configurations. Random numbers are used to vary the input values. The results are presented.

Keywords

Liquid Rocket Propulsion — Turbopump — Axial Thrust — Radial Forces

[1] *Institute of Space Propulsion, German Aerospace Center (DLR), Lampoldshausen, Germany*

[2] *Technical University of Munich, Department of Mechnical Engineering, Chair of Turbomachinery and Flight Propulsion, Division Space Propulsion, Munich, Germany*

*__Corresponding author__: bernd.wagner@dlr.de

INTRODUCTION

In modern liquid propellant rocket engines (LRE) turbopumps (TP) are inevitable to provide the combustion chamber with a high propellant massflow at high pressure. Both are necessary for the performance of the engine and an efficient, lightweight stage e.g. due to a low tank pressure, thus a reduced structure weight. In order to meet the engine requirements in terms of performance the turbopump assembly (TPA) must be able to operate at high speed, work over a wide operational range, and has a high power density. Depending on the configuration and the possible engine cycle, a TPA consists of inducers, pumps, turbines, a seals, bearings, and shaft system, and a housing with flanges. Each part is designed to operate under harsh boundary conditions and with a low system weight. In order to minimize the stresses on heavily loaded parts like the bearings, the forces acting in radial and axial direction should be estimated. Furthermore, during the design process of the TP parts, the balance of the axial forces can be achieved. Therefore, the aerodynamic and hydraulic forces acting on each part of the TPA have to be calculated and brought into relation. The results are an important starting point for further design details and first rotordynamic analysis.

1. PROJECT BACKGROUND

The project KonRAT has been initialized 2015 as part of the national effort to build up further competencies in turbomachinery technology for LRE. KonRAT is a German abbreviation for application of rocket propulsion components for aerospace transport systems. Key objectives of this project are establishing design procedures for TP for cryogenic oxygen, investigations on selected problems in turbopumps and, finally, additive manufacturing methods for aerospace applications like turbopump parts and rocket engine valves. The turbopump branch of the project is mainly performed at the Technical University of Munich, for more information see [1]. The work on TP includes state of the art design procedures [2, 3]. In a newly erected test bench measurements with heated water are performed for TP components [4]. Experimental and numerical observations on seals and bearing and their influence on the rotordynamic are also ongoing [5, 6]. Detailed analysis of seal and bearing elastohydrodynamic are performed with sophisticated fluid structure interaction solvers. The DLR contributes to the project with observations on secondary flows, including the axial and radial forces resulting from these flows.

Two baseline configurations are considered in the project. First, a future upper stage in the 120 kN class for launchers is investigated, second, a main stage engine for sub-orbital flight vehicle. The configurations are summarized in table 1.

Table 1. Applications of the KonRAT project

Application	Launcher	Sub-orbital vehicle
Type	Upper stage	Main stage (boost)
Cycle	Expander	Gas generator
Fuel combination	LH2/LOx	LCH4/LOx
Thrust /t	11-15	40-50
Specific impulse /s	>450	>340

2. CALCULATION OF ACTING FORCES

The major part of the forces on the bearings is caused by the pressure forces acting on the outer walls of flow surrounded rotating parts. In addition, forces and moments come from momentum and weight, as well as vibrations, unbalance and disturbances in the flow. The used methods to calculate these forces are briefly presented here.

2.1 Axial Thrust

First, reference is made to the axial loads, also called axial thrust or force, which is produced by the inducers, the impellers and the turbines. Simple ways to estimate these forces are shown here for no flow through configurations. The axial forces have two causes. First, forces are caused by the deflection of the flow as an impulse force on the side walls of the rotating components, which can generally be formulated

$$dF = \frac{d}{dt}(dm \cdot c). \tag{1}$$

Second, pressure forces act on the side walls, which are described as follows for axis-symmetric cases

$$F = 2\pi \int prdr. \tag{2}$$

From this, the axial forces can be derived from the pressure distribution of surfaces of all the individual components.

2.1.1 Inducer

Typically, inducers are installed in liquid rocket turbopumps, which have a pure axial construction without a shroud. They are therefore to be treated as axial rotors, for which the axial force can be determined by

$$F_{ax,in} = \frac{\pi}{4}(d_2^2 - d_n^2)\rho g H_{in} \tag{3}$$

In Gülich [7] this equation is additionally multiplied by a correction factor between 1 and 1.1. In case the inducers are equipped with a variable diameter an impulse change of the flow and the resulting force on the inducer can be considered. However, this additional force is very low compared to the other forces and is ignored here.

2.1.2 Impeller

The axial forces acting on the impeller are again composed by impulse forces and pressure forces acting on the outer walls of the impeller. Here, only the case of a wheel side wall which is not flowed through is to be considered. This is an acceptable simplification for the design considerations discussed here. According to Gülich [7] from equation 2 the forces on the hub and shroud of the impellers can be determined in the axial direction with

$$F = \pi r_2^2 \left[\left(1 - x^2\right) \Delta p_{imp} - \frac{\rho}{4} u_2^2 \bar{k}^2 \left(1 - x^2\right)^2 \right] \tag{4}$$

Where x is the respective ratio between the inner and outer diameters of the impeller side wall, and k is the average rotational factor. The geometrical influences on the pressure profile acting on the side wall are mainly introduced by this factor. Since in the present case exclusively no flow through is considered in the rotor stator cavities, the rotation factor can be expressed by

$$\begin{aligned} k_0 &= \frac{1}{1 + \sqrt{\frac{A}{B} * \left(\frac{c_{f,w}}{c_{f,imp}}\right)}} \text{with} \\ A &= \frac{1}{\cos\delta_w}\left[\left(\frac{r_w}{r_2}\right)^5 - \left(\frac{r_i}{r_2}\right)^5\right] + 5\frac{t_{ax}}{r_2}\left(\frac{r_w}{r_2}\right)^4 \\ B &= \frac{1}{\cos\delta_R}\left[1 - \left(\frac{r_i}{r_2}\right)^5\right] + 5\frac{t_{ax}}{r_2}\left(\frac{r_i}{r_2}\right)^4 * \\ &\quad \left[1 + \frac{r_w - r_i}{t_{ax}}\tan\delta_w - \frac{r_2 - r_i}{t_{ax}}\tan\delta_R\right] \end{aligned} \tag{5}$$

If the angles α between the side walls of the impeller and the housing side walls are neglected and r_i is small compared to the impeller radius r_2, equation 5 is simplified to

$$k_0 = \frac{1}{1 + \left(\frac{r_w}{r_2}\right)^2 \sqrt{\left(\frac{r_w}{r_2} + 5\frac{t_{ax}}{r_2}\right)\frac{c_{f,w}}{c_{f,imp}}}} \tag{6}$$

The impulse force is also very small for the impeller and is calculated by

$$F_{imp} = \rho Q c_{1m}. \tag{7}$$

Depending on the installation situation, the static pressure at the impeller inlet and the unbalanced shaft thrust over the entire turbopump can also be considered. Axial forces resulting from small pressure affected surfaces and seals are neglected in this preliminary study.

2.1.3 Turbine

For the calculation of the forces acting on the turbine a general approach is applied in order to meet the possible configurations of the turbines. This includes the two causes of the acting forces from equations (1) and (2) and is formulated as

$$F_{ax,t} = \frac{\pi \alpha_{part}}{360^\circ} \left[(p_1 - p_2) + (c_{1,ax}^2 \rho_1 - c_{2,ax}^2 \rho_2) \right]. \quad (8)$$

A partial admission inflow of the turbine can be taken into account by the angle α_{part}. This would cause an additional moment on the shaft. Equation 8, however, represents only an estimation of the forces, a more precise determination of axial forces acting on the turbine disks should be carried out with numerical flow solvers like for example in Dorney [8].

2.2 Radial Forces

Since the flow in turbopumps is axis-symmetrical, most of the forces acting in the radial direction are mutually compensated. Radial forces are only caused by a disturbance of rotational symmetry. In the following, a difference is made between stationary forces, whose effective direction is determined by the geometry of the turbopump, and dynamic forces.

The major part of the radial loads acting on an impeller is usually produced by the spiral-shaped outlet at the last stage. It can be calculated as follows:

$$F_R = k_R \rho H d_2 b_{2,ges} \quad (9)$$

Where $b_{2,ges}$ is the width of the impeller at the outlet, including the hub and shroud wall thickness. The radial thrust coefficient k_R can be estimated according to Stepanoff [9] with

$$k_R = 0.36 \left(1 - \frac{Q}{Q^*} \right). \quad (10)$$

In this case the radial force acts in the direction of a point which lies approximately 60° downstream of the housing tongue when partial load is reached. The maximum value of k_R was used for the calculation in the program. More detailed methods for the calculation of the radial forces in spiral housings like e.g. from Domm and Hergt [10] are not yet taken into account and will be implemented in the future.

2.3 Weight Forces - Gravitation

Even if the proportion of the weight forces at the acting axial and radial forces is quite small, it is calculated in the following form.

$$\begin{aligned} F_{g,x} &= -m(g+a)\sin\alpha_w \\ F_{g,y} &= -m(g+a)\cos\alpha_w. \end{aligned} \quad (11)$$

In addition to the gravitational acceleration g, the lift-off acceleration a of the launcher or of the stage can also be added. The mass m is determined individually on the basis of the given dimensions and material for each component, but it can also be input directly if precise values are known from CAD models. Typically, turbopumps are installed at an angle of 90° or 270° to allow the pumps to be fed in the direction of acceleration. More rarely is a horizontal arrangement which means in the convention in here: 0° or 180°.

2.4 Dynamic Forces - Unbalance

The equations above consider only steady-state forces. During the operation of rocket engine turbopump strong dynamic loads also affect the rotor. Vibration and acoustics loads emerging from the engine and the rocket structure act from outside on the turbopump. The turbopump itself is exposed to hydraulic and aerodynamic vibrations which couples with rotordynamics and unbalance vibrations. The direction of action and/or the magnitude may change considerably over time. Most of these vibrations and forces are difficult to assess analytically in the preamble in a precise way. However, for forces caused by unbalance (mass asymmetry), an experimentally proven first formula for well-balanced, fast-rotating runners can be found in [11] as

$$F_{un} = (0.02...0.04) d_2 m n^2. \quad (12)$$

0.04 was used in the program as prefactor, whereby the calculated unbalance forces are strongly overpredicted. The general application of this equation for the fast-rotating components in space propulsion drives is not entirely clear and variation of this factor has a linear impact on the prediction of dynamic forces due to unbalance.

3. APPLIED METHOD

3.1 Program for Axial and Radial Forces

A tool has been developed to estimate the forces acting on inducers, impellers, and turbines in both axial and radial directions. The calculation of forces acting on the hydraulic parts in axial direction are based on Gülich [7], where the impulse, pressure forces acting on hub and shroud, and unbalanced axial force on shaft are considered for no flow through at a first step. Radial forces are determined only for the volute with a simple method proposed by Stepanoff [9]. Aerodynamic forces on the turbine are estimated considering impulse forces and if present pressure difference. Additional moments due to partial admission of the turbine can be taken into account, too. Forces due to unbalance of the parts are roughly evaluated. Finally, the weight of each part is calculated depending on the orientation of the TP in the engine and the acceleration of the rocket stage. Based on the dimension and position of the parts, the resulting bearing forces are calculated.

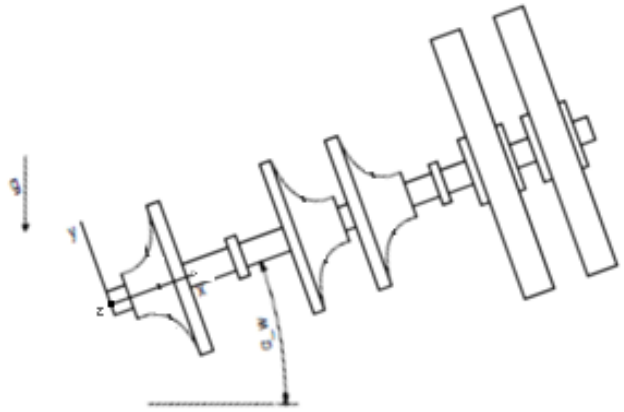

Figure 1. Example of turbopump configuration

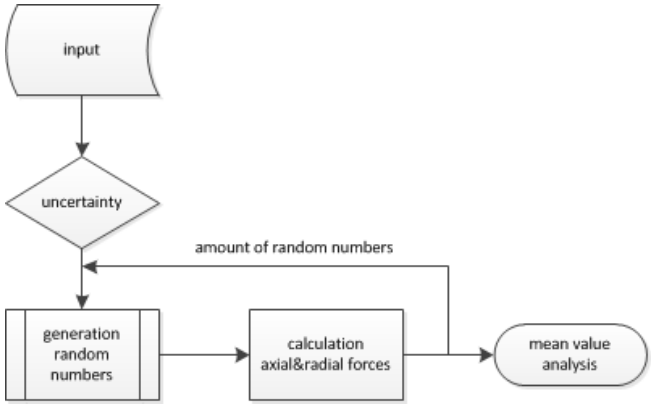

Figure 2. Flow chart for random number generation

The different configurations of existing TPAs have been evaluated in a small literature review and the tool is able cover most types of modern TPA featuring inducer, up to three stage impellers for both oxidizer and fuel pumps together with a maximum of a three stage turbine on one shaft. In figure 1 an example of a possible TP configuration can be seen. The convention, which is used for the acceleration and orientation, can also be found there.

3.2 Variation of Input Values

A main feature of the tool is the generation of random numbers to take the uncertainties of performance values into account. This Monte Carlo like approach is necessary in an early stage of design. Each input value for the calculation of the forces can be provided with a certain range of uncertainty. The main difference to a classical Monte Carlo method is, that the set of random number is created with the following Gaussian distribution.

$$f(x) = \frac{1}{\sigma\sqrt{2\pi}} e^{-\frac{1}{2}(\frac{x-\mu}{\sigma})^2} \tag{13}$$

The cycle of random number generation is shown in figure 2b. The uncertainties can be set globally, but also individually to accommodate the detailing and reliability of the input values. This function can also be used to assess the influence of input values on the entire design. A detail description of the tool can be found here [12]. An enhancement of the tool is the interface to a simple bearings stiffness tool based on a general theory for elastically constrained bearings [13] and the generation of input values for a dry rotordynamic analysis, which can be started directly from the tool.

The statistical procedure has been implemented instead of an analytical evaluation for the following reasons:

- Keep the tool very flexible and allow individual adjustments during the design process
- Provide probability curves of the loads for the bearing design
- Being open to flow through observations with differential equations.

4. RESULTS AND DISCUSSION

The method has been applied during the design of a liquid rocket expander cycle upper stage engine LOx turbopump with roughly 120 kN thrust. The design methods and configuration of this TP are described in Veggi [14], it is an alternative design approach to the work of Maeding and Souverein [15, 16].

Table 2. LOx turbopump nominal operating conditions

Property	Value	Unit
Rotational speed N	20000	rpm
Nominal mass flow rate $\dot{m}$	25	kg/s
Total pressure at pump inlet $p_{t,1}$	2.5	bar
Temperature at pump inlet T_1	90	K
Total pressure at pump outlet $p_{t,3}$	70	bar

The 120 kN turbopump consists of an inducer, an impeller, a fixed bearing, the sealing unit, a loose or floating bearing and a turbine, all together on one shaft. For the calculations the design values are available and a direct interface to design tools has been implemented. The dimensions for bearing, seal, and shaft were estimated based on experience.

4.1 Forces Acting on the Bearings

According to previous investigations [12], a setting of one hundred thousand random numbers, which leads to converged solution, and a global deviation from the input values of 20 % was used. This strong deviation is certainly very conservative. The two bearings are viewed separately from each other. In the present case, the fixed bearing is assigned to the pump, the floating bearing to the turbine. An inverted configuration could also be possible.

Figure 3 shows the histogram of values of the bearing forces acting on the fixed and loose bearing. All results are

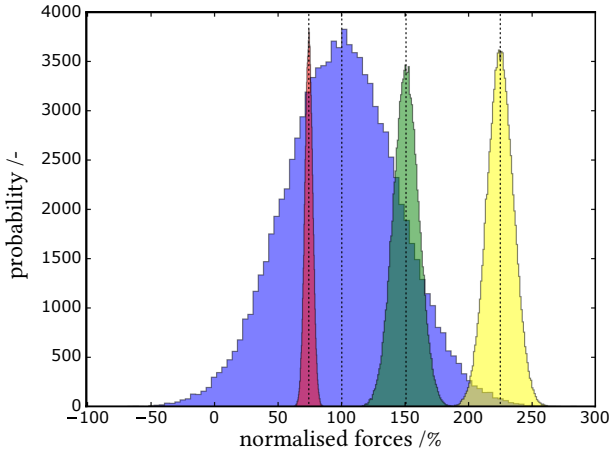

(a) Fixed bearing

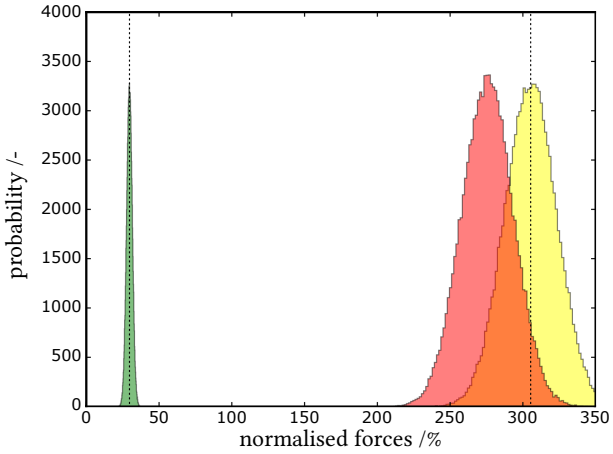

(b) Loose bearing

Figure 3. Results of bearing loads normalised by axial forces (blue), radial forces statically (green), dynamic radial forces (red), combined radial forces (yellow)

normalised by the mean value of the axial force. The wide range of the axial force results mainly from the large number of input parameters to the calculation, which are all varied. In the present case of 20 % variation values of axial forces with negative signs can occur. Thus, the direction of loads on the bearing would change. Frequent changes would increase the load on the bearing and limit the lifetime. Therefore, these cases should be avoided at any time.

Radial forces are also shown in figure 3. In the fixed bearing (top figure), the static radial force are mainly caused by the spiral housing. The forces are in the same order of the axial force. This results in a balanced discharge of force into the bearing when, for example, angular contact ball bearings are used. The dynamic radials loads are plotted in red and they are half of the radial once. They result from the expected unbalance of the rotating mass of the inducer, impeller, and partly the shaft according to equation 12. However, the total estimated radial force, thus, the sum of the proportions of the static and dynamic forces are shown in yellow.

The loose bearing, in contrast, shows a different behavior. The fraction of dynamic forces is very high, as it can be seen in figure 3(b). The loose bearing is situated close to the turbine and the assumed unbalance of the turbine disk according to equation 12. The high rotational speed, the large diameter and the necessary mass lead to these high values. Up to now, the turbine disk design is not fixed yet. Therefore, the mass is estimated within the program. A constant shear stress profile is assumed and defines the width of the disk depending on the radius. From this derived geometry, the mass can be calculated for high strength steel. In the present case of 120 kN engine, the turbine is designed as full admission turbine. Thus, the turbine with its axis-symmetric inflow does not create static radial forces or moments on the rotor. The acting forces on the floating bearing results from the volute forces and are transferred by bending. Hence, their portion is very small.

4.2 Variation of Parameters

The results in figure 3 show already the capability of the program to use random numbers for the calculation of axial and radial forces. Due to uncertainties in the prediction of the input values for the estimation of those forces, this procedure was chosen. During the design and development process, more precise values will be available and the variation of random number can be individually adapted and/or generally lowed. In the following sections the influence of both procedures will be discussed.

4.2.1 Global Variation

20 input values in the equations 3 to 12 can currently be varied in the program. This includes also the mass of the rotating parts. In this section the global setting for the deviations in standard distribution in equation 13 is varied for the axial forces.

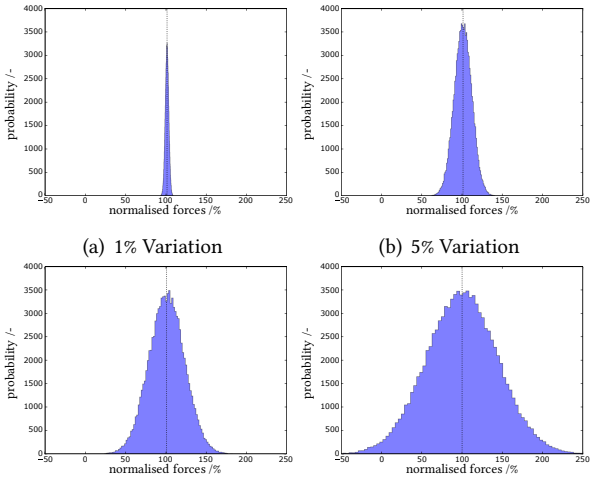

(a) 1% Variation (b) 5% Variation

(c) 10% Variation (d) 20% Variation

Figure 4. Influence of variation on axial forces

Results for four different global settings of uncertainties are presented in figure 4. The impact of the different values for the variation is clearly visible. A variation of 10 % already

lead to a three σ deviation of more than 50 % for the axial thrust. In a comparison performed by Beck [17] between simulations and the results of equation 4 for a LOx TP with comparable dimensions, the offset ranged between 10 % to 17 %, depending on the geometrical conditions of the rotor stator cavity without flow through. Therefore, 10 % variation in the values are not unlikely and the 20 % variation can be treated as an extreme case.

4.2.2 *Individual Variation*

After the global variation of the 20 values the influence of variation of each value is studied. Following procedure is applied for this assessment. Each values is individually varied while keeping the other values constant as the input value and then the next value is varied. For each calculation the three σ value of the forces on both fixed and loose bearing is recorded and plotted. Now, the forces are normalised by the mean value in order to visualise clearly the deviations.

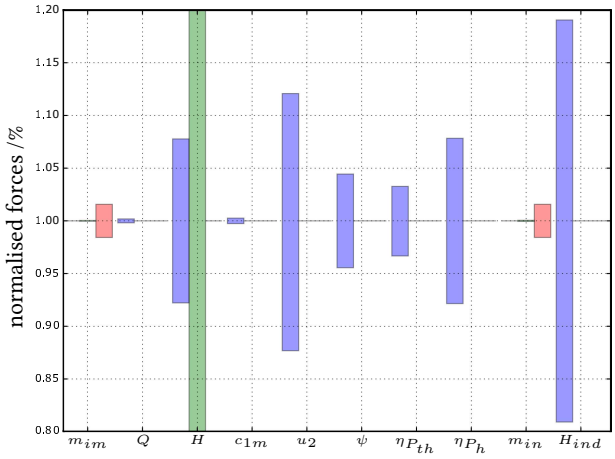

(a) Part I

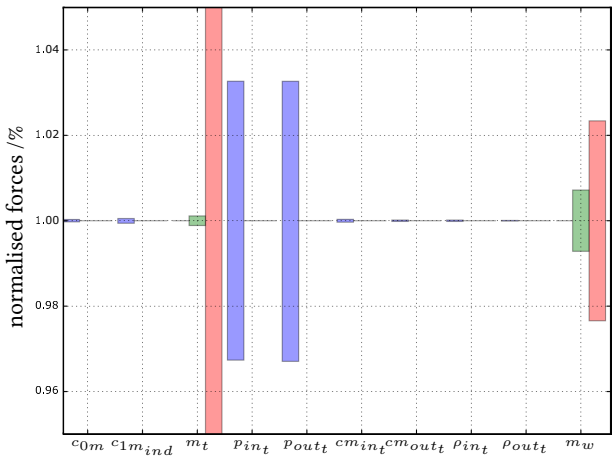

(b) Part II

Figure 5. Results of normalised bearing loads on the fixed bearing for individual variation of input values, axial forces (blue), static radial forces (green), dynamic radial forces (red)

In figure 5 the results of this study are shown for the fixed bearing. It should be noted that a different scale has been used for figure 5a, because the impact is higher there and greater values occur. Considering the axial thrust, the head of inducer and impeller have a strong impact. The other values for equation 4 also influence the axial force strongly. The variation of the pressure ratio, here as two pressure values (p_{in_t} and p_{out_t}) through the turbine contributes to the axial thrust. Some minor influence is given by the volume flow Q. In case of static radial forces, there is a strong dependence on the head rise H which can be seen from equation 9. The geometrical values are kept constant for the estimation of the radial forces due to the volute around the impeller. The mass of the parts has some contribution to the radial forces, too. Their influence on the dynamic forces can been seen in the red bars, where up to now only unbalance is considered.

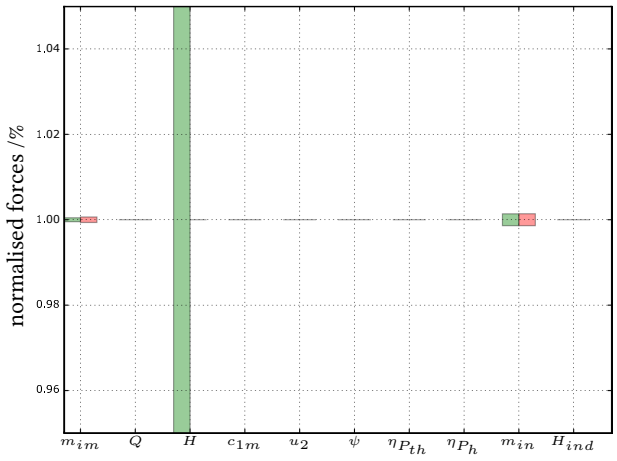

(a) Part I

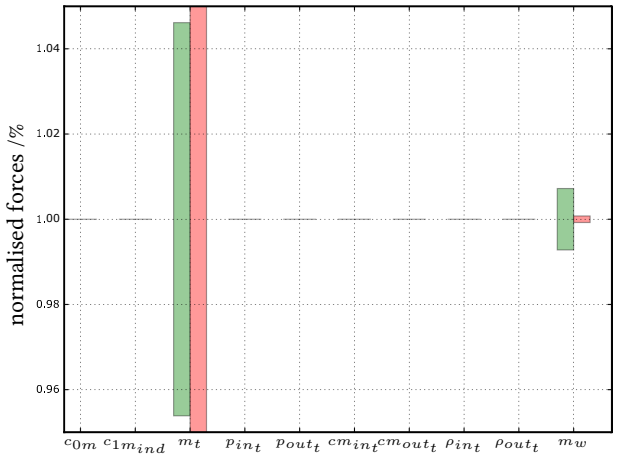

(b) Part II

Figure 6. Results of normalised bearing loads on the loose bearing for individual variation of input values, radial forces statically (green), dynamic radial forces (red).

The results for the loose bearing are shown in the two graphics of figure 6. Of course, there is no contribution to axial forces. The static radial force mainly results from bending and are transfered via the shaft from the volute. In the 120 kN turbopump, the loose bearing is close to the turbine.

Therefore, the unbalance forces resulting from the variation of m_t are very high. In figure 6, the values of exceed the scale of the y-axis. This visualisation was chosen on purpose so that the values of the other results are still in a reasonable size.

5. CONCLUSION

A program was developed to calculate the bearing forces in turbopumps of liquid rocket engines. It is applicable to most turbopump configurations. This was confirmed by intensive literature research on turbopump designs. The operation of the program and results were discussed with a LOx turbopump for a 120 kN upper stage engine. The results are influenced by two areas. On the one hand, the input values for the program depend on the quality of the design of the hydraulic and aerodynamic components, on the other hand, the validity and precision of the equation used for estimating the acting forces. Both uncertainties were taken into account by the generation of random numbers around the input values with a given variation. The variance was adapted individually in order to investigate the influence on the resulting forces. The input values become more precise through each design loop. Numerical simulations and experiments can also be used to prove both the empirical equations used and the input values and, if necessary, further adapt them. The presented considerations represent only one area in the investigations on secondary systems and are only one aspect in the selection of the turbopump configuration. With regard to the bearing forces, several points have to be mentioned which have a strong influence on the results and the configurations, but have not been taken into account here:

- Calculation of impeller side walls with regard to superimposed flow
- Adjustments by axial thrust compensation
- Observations outside the nominal operating point
- Stiffness of ball bearings due to the distribution of forces
- Consideration of rotordynamic effects

Work on these points is already taking place. For example, a module to deal with superimposed flow in the rotor stator cavity is available and has been validated against numerical simualtions. It has been applied on active axial thrust balancing in LRE TP [18]. An integration and loosely coupling of programs for the calculation of bearing stiffness and / or rotordynamic natural frequencies of the turbopump have also already been implemented and tested. The secondary systems remain an interface between the disciplines working on the turbopump design and contribute to the improvement of the entire system.

NOMENCLATURE

Abbreviations

DLR	German Aerospace Center - Deutsches Zentrum für Luft- und Raumfahrt
LOx	Liquid oxygen
LRE	Liquid Rocket Engine
TP	Turbopumps
TPA	Turbopumps Assembly
TUM	Technical University of Munich

Symbols

α	Angle between impeller side walls o and the housing
α_w	Orientation of turbopump
μ	Mean of distribution
ρ	Density
σ	Standard deviation
$b_{2,ges}$	width of impeller at outlet
c_{1m}	Meridian velocity inflow
c_f	Skin friction coefficients
a	Launcher or stage acceleration
c	Absolute velocity
d	Diamter
F	Force
g	Gravitational acceleration. $g = 9.81 m/s^2$
H	Head rise
k	Average rotational factor
m	Mass
n	Rotational speed
p	Pressure
Q	Volume rate
r	Radius
t	Axial clearance
u	Circumferential speed
x	between the inner and outer diameters

Subscripts

2	At impeller outlet

ax	Axial
imp	Impeller
in	Inducer
R	Radial
t	Turbine
un	unblance
w	Housing wall
w	Shaft

ACKNOWLEDGMENTS

The KonRAT project within the Ludwig Bölkow Campus is funded by the Bavarian Ministry of Economic Affairs and Media, Energy and Technology under grant number: LABAY83E. This financial support and the good cooperation between the project partners is gratefully acknowledged.

REFERENCES

[1] J.D. Pauw et al. Untersuchungen zu Turbopumpen an der Technischen Universität München im Rahmen des KonRAT Projekts. In *Manuscript submitted to 66th DLRK for publication*, München, Germany, 2017.

[2] L. Veggi, J.D. Pauw, B. Wagner, and O. J. Haidn. A study on the design of LOX turbopump inducers. In *Manuscript submitted to ISROMAC for publication*, Maui, HI, USA, 2017.

[3] L. Souverein, L. Veggi, S. Sudhof, R. Behr, and O. Haidn. On the effect of axial turbine rotor blade design on efficiency: a parametric study of the Baljé-diagram. In *7th European Conference for Aeronautics and Space Sciences*, 2017.

[4] J.D. Pauw, L. Veggi, B. Wagner, J. Mondal, M. Klotz, and O. J. Haidn. Design procedure of a turbopump test bench. In *Manuscript submitted to ISROMAC for publication*, Maui, HI, USA, 2017.

[5] Ch. Wagner, T. Berninger, T. Thümmel, and D. Rixen. Rotordynamic effects in turbopumps for space propulsion systems - first minimal models and experimental validation. In *5th Conference on Space Propulsion*, 2016.

[6] Ch. Wagner, B. Proux, A. Krinner, T. Thümmel, and D. Rixen. Rotordynamik: Modellierung und einfluss von schrägkugellagern für hochdrehzahlanwendungen. In *Second IFToMM D-A-CH Conference*, 2016.

[7] J. F. Gülich. *Centrifugal Pumps*. Springer, 2 edition, 2010.

[8] D. J. Dorney, B. Marcu, K. Tran, and S. Sargent. Calculation of turbine axial thrust by coupled CFD simulations of the main flow path and secondary cavity flow in an SLI LOx turbine. In *39th AIAA/ASME/SAEI/ASEE Joint Propulsion Conference and Exhibit*, number AIAA 2003-4919, 2003.

[9] A. Stepanoff. *Radial- und Axialpumpen. Theorie, Entwurf, Anwendung*. Springer Verlag, 1957.

[10] U. Domm and P. Hergt. Radial forces on impeller of volute casing pumps. 1970.

[11] H. Sigloch. *Strömungsmaschinen. Grundlagen und Anwendungen*. Hanser Verlag, 2013.

[12] B. Wagner, A. Stampfl, P. Beck, L. Veggi, J.D. Pauw, and W. Kitsche. Untersuchungen zu Sekundärsystemen in Turbopumpen für Flüssigkeitsraketenantrieben. In *65. Deutscher Luft- und Raumfahrt Kongress*, 2016.

[13] A. B. Jones. A general theory for elastically constrained ball and radial roller bearings under arbitrary load and speed conditions. 82(2):309–320, 1960.

[14] L. Veggi, J. D. Pauw, B. Wagner, T. Godwin, and O. Haidn. Numerical and experimantal activities on liquid oxygen turbopumps. In *5th Conference on Space Propulsion*, 2016.

[15] C. Maeding, L. Souverein, D. Hummel, S. Koenigbauer, A. Wagner, and J. Alting. A preliminary design study for an expander LOX turbopump. In *6th European Conference for Aeronautics and Space Sciences*, 2015.

[16] L. Souverein, C. Maeding, T. Aichner, B. Ivancic, A. Wagner, and M. Frey. Design and tool anchoring for a 120kN expander cycle rocket engine LOX turbopump. In *6th European Conference for Aeronautics and Space Sciences*, 2015.

[17] P. Beck, B. Wagner, and O. Haidn. The influence of secondary flow in the thrust acting on the axis of a radial lox pump. In *Proceedings of 12th European Conference on Turbomachinery Fluid Dynamics and Thermodynamics*, 2017.

[18] S. Maier, B. Wagner, L. Veggi, J.D. Pauw, and P. Beck. Analytical and numerical assessment of axial thrust balancing systems in liquid rocket engine LOx turbopumps. In *7th European Conference for Aeronautics and Space Sciences*, 2017.